INVESTIGATING ANNULAR FLOWS AND THE EFFECT OF FUNCTIONAL SPACERS IN AN ADIABATIC DOUBLE-SUBCHANNEL MODEL OF A BWR FUEL BUNDLE BY ULTRA-FAST X-RAY TOMOGRAPHY

R. Zboray¹, M. Guetg³, J. Kickhofel³, F. Barthel², U. Sprewitz², U. Hampel², H.-M. Prasser^{1,3}

¹ Paul Scherrer Institut, PSI Villigen, Switzerland

² Helmholtz-Zentrum Dresden-Rossendorf, Dresden, Germany

³ ETH Zürich, Swiss Federal Institute of Technology, Zürich, Switzerland

robert.zboray@psi.ch*

Abstract

Dryout of the coolant liquid film at the upper part of the fuel assemblies of a boiling water reactor (BWR), where annular flow prevails, represents a safety concern and an economical constraint. To be able to deal with this issue, annular flows must be well understood. Therefore, we have investigated such flows in a double-subchannel model of a BWR fuel bundle using X-ray imaging at the Rossendorf Ultrafast Electron Beam X-ray Tomograph (ROFEX) facility. Adiabatic experiments somewhat above atmospheric conditions using air-water annular flows have been carried out. In annular flows a significant portion of the liquid is present as droplets in the gas flowing in the middle of the conduit. Using functional spacer grids is the common method in nuclear technology to influence the annular flow as to enhance the deposition of droplets into the liquid film on the fuel pins, thereby increasing dryout margins. The tests include, besides investigating the liquid film thickness in the plain channel, the investigation of the effect of a functional spacer on the liquid film. Using NaI as contrast agent in water enhances the image quality. The high time-resolution of the tomography enables measuring of the wavy structure of the annular film flow. The paper aims at extracting quantitative information on the liquid film thickness distributions from the reconstructed tomographic images.

Introduction

At the upper section of boiling water reactor (BWR) fuel assemblies, the dominant flow regime is annular flow of the coolant and as long as the water film is present on the surfaces of the fuel pins a sufficient heat transfer from the fuel pins can be maintained [1]. If the heat transfer abruptly diminishes, e.g. due to dry out of the film, a sharp rise in the fuel pin temperature takes place; a so called boiling crisis occurs. Such crisis endangers the integrity of the fuel and thus clearly represents a safety concern. The maximum allowed specific enthalpy growth of the coolant, characterized by a critical equilibrium thermodynamic quality, is limited by the dryout, which in turn also limits the thermal power output of a BWR [1]. Note that there is another type of boiling crisis at low-quality conditions mostly relevant for Pressurized Water Reactors (PWR) occurring at a so-called critical heat flux (CHF), however the present study focuses on the aforementioned high-quality, high-void fraction annular flow regime in a fuel-bundle geometry. Annular flow is characterized by the presence of a continuous liquid film flowing on the channel wall surrounding a central gas core laden with liquid droplets entrained from the liquid film. The gas-liquid interface is very dynamic with very erratic waves traveling on it. The literature usually distinguishes between large

_

^{*} Corresponding author

disturbance waves and relatively small-wavelength and small-amplitude ripple waves traveling at much lower velocity compared to the velocity of the disturbance waves and of the gas phase [22]. The thickness of the liquid film is an important parameter for the thermal hydraulic behavior around the fuel pins in a BWR. However, in the annular flow regime a significant portion of the coolant might be in the form of droplets in the vapor core not contributing to the cooling of the fuel pins. The atomization of the large disturbance waves by the turbulent gas core is believed to be the main source of droplet entrainment into the core of the annular flow [22]. Promoting droplet deposition onto the liquid film is one potential way to enhance liquid film thickness (LFT) and dryout margins. This can be done by using functional spacers: spacer grids enhance the stability of the fuel pins while spacer vanes are used to influence the flow. The main requirements for BWR spacers are that they provide a maximal efficiency in phase separation to transfer droplets onto the fuel rods while they induce a minimal pressure drop. A vast number of patents and proprietary designs exist for different types of spacers e.g. [2], [3], [4], [5]. BWR fuel vendors have put great efforts into improving fuel spacers in order to obtain better performance from their fuel assembly. For example, the ULTRAFLOWTM spacers developed for the different types of ATRIUMTM fuel assemblies by AREVA [6], [7], [8], [9].

Earlier research has confirmed the basic benefit of spacer vanes in enhancing the liquid film thickness and thus the dryout margin [6], [7], [10]. Nevertheless, the mechanisms by which the spacers affect the annular flow and film thickness are still subject to debate and might depend strongly on the actual grid and vane geometry. The dominating effects for promoting droplet deposition may include the direct disturbance of the spacer on gas flow, diffusing droplets laterally, turbulence promotion, and the run-off of droplets from the spacer surface [11]. For nuclear fuel assembly development there is a strong need for experimental techniques that could be used to obtain detailed information on functionality of different spacer designs. Numerous experimental techniques have been tested and developed to study annular flows. These include intrusive methods, however much more popular are non-intrusive techniques mostly based on conductance or capacitance measurement, e.g. [7], [12]. Damsohn & Prasser [10], [12] have developed a conductivity-based liquid film sensor (LFS) capable of a 10 kHz sampling rate at a spatial resolution of 2 mm. Non-intrusive imaging techniques based on e.g. neutron tomography are also increasingly applied [13], [14], [15], [16].

We have used a model of two neighboring subchannels of a BWR fuel bundle and examined adiabatic, air-water annular flows in it by ultra-fast X-ray imaging. It is a scaled-up (about 1:2) double-subchannel model with respect to actual BWR bundle and it has been previously used to investigate annular flows and spacer effect by two other techniques, namely LFS [12] and cold neutron tomography [10], [15] and [16]. The former one is time-resolved, its spatial resolution is somewhat limited. The latter provides only time-averaged results but at a higher spatial resolution. The ultra-fast X-ray tomograph used for the present study offers an interesting alternative to the two aforementioned techniques. It has a high time resolution and a spatial resolution that might enable examining annular flows when the liquid film is reasonably thick. Furthermore, the ultra-fast X-ray tomography has been used extensively for imaging bubbly and slug flows [19], [20], however its ability for resolving annular flows has not yet been investigated in detail. The latter is the goal of the present study to see if it is feasible to obtain quantitative information on annular flow parameters like e.g. the distribution of liquid film thickness or the wave structure of the liquid film. This is examined and shown below based on a few selected experiments.

1. Experimental setup

1.1 Two-phase flow loop

A simple and compact two-phase flow loop and auxiliary equipment have been used. The setup consists of a closed water loop and open loop of dry air joining at the base of the channel as is shown in Figure 1. After the multiphase mixture leaves the double subchannel that is at the heart of the loop, it is led to a tank where the air is exhausted while the water is recycled by a pump. Air and water flows are measured by vortex flowmeters. The absolute pressure in the channel is measured at its base near the air inlet. Flexible inlet and outlet hosing is used to enable fitting the channel in to the tomograph.

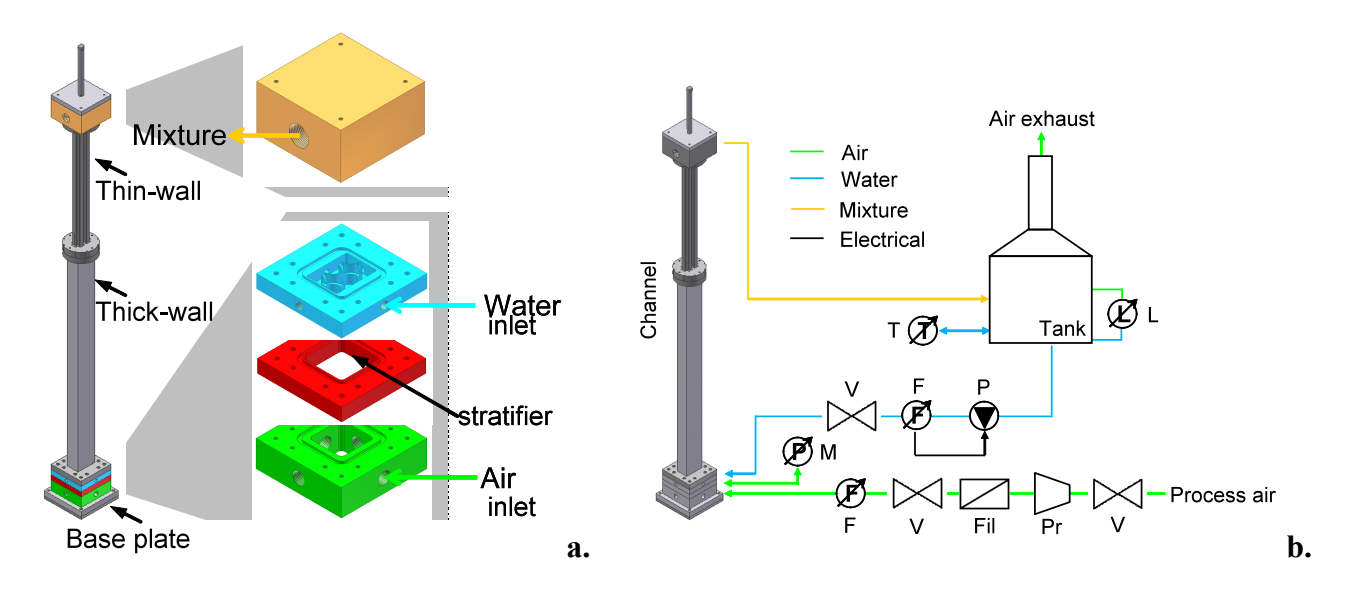


Figure 1 Scheme of the double subchannel (a) and the two-phase flow loop with it (b).

The channel has been previously used for cold neutron imaging, therefore, it is made of aluminum. It comprises a thin-wall (3 mm thickness) upper section and a thick-wall lower section as is shown in Figure 1. Imaging is always performed at the thin-wall section. The base of the channel comprises a base plate, four air inlets, a flow stratifier and four water inlets (one each side) as is shown in Figure 1a. The channel accomplishes the introduction of air, stratification in a honeycomb grid and the injection of water in 8 vertical centimeters. The water inlet piece is designed specifically to inject the liquid at the walls using beveled edges such that the flow is already near-annular at the inlet, see [10] for details. The incoming air and water flow are each split into four inlet connections, respectively, evenly distributing water around the double subchannel inlet geometry while minimizing air pressure drop. The flow is provided approximately 90 cm to develop in the double subchannel before reaching the spacer vanes and another 42 cm downstream before reaching the outlet. The cross section of the double subchannel is shown in Figure 2. It is confined by walls simulating 4 quarter and 2 half virtual fuel pins. This represents a kind of minimal geometry where the two half pin surfaces are relatively undisturbed by the confined geometry and it requires significantly lower air and water flow rates than a larger multi-pin bundle.

Two spacer designs have been investigated in this work. Both are similar to spacers used in industrial applications and are shown in Figure 3. Spacer 1 is a ferrule-type spacer design, while Spacer 2 comprises split vanes that have been developed in the context of low-quality CHF

problems to promote crossflow between subchannels. The 3 cm tall spacer grids reside between 2 and 5 cm from the start of the thin-wall section. These spacers have been constructed out of 0.5 mm thick aluminum sheets laser welded together. Two thin 1.5mm wide and 2mm deep grooves are present in the first 5 cm of the thin-wall section (see Figure 2) and act as a positioning system for the spacers while inflicting minimal impact on the flow.

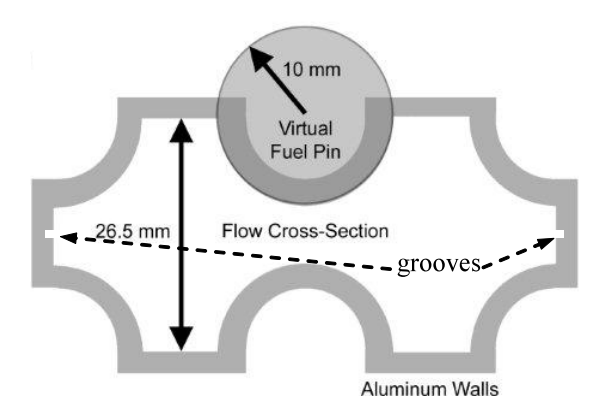


Figure 2 The cross section of the double subchannel. Note that the grooves are only present in the first 5 cm of the thin-wall piece.

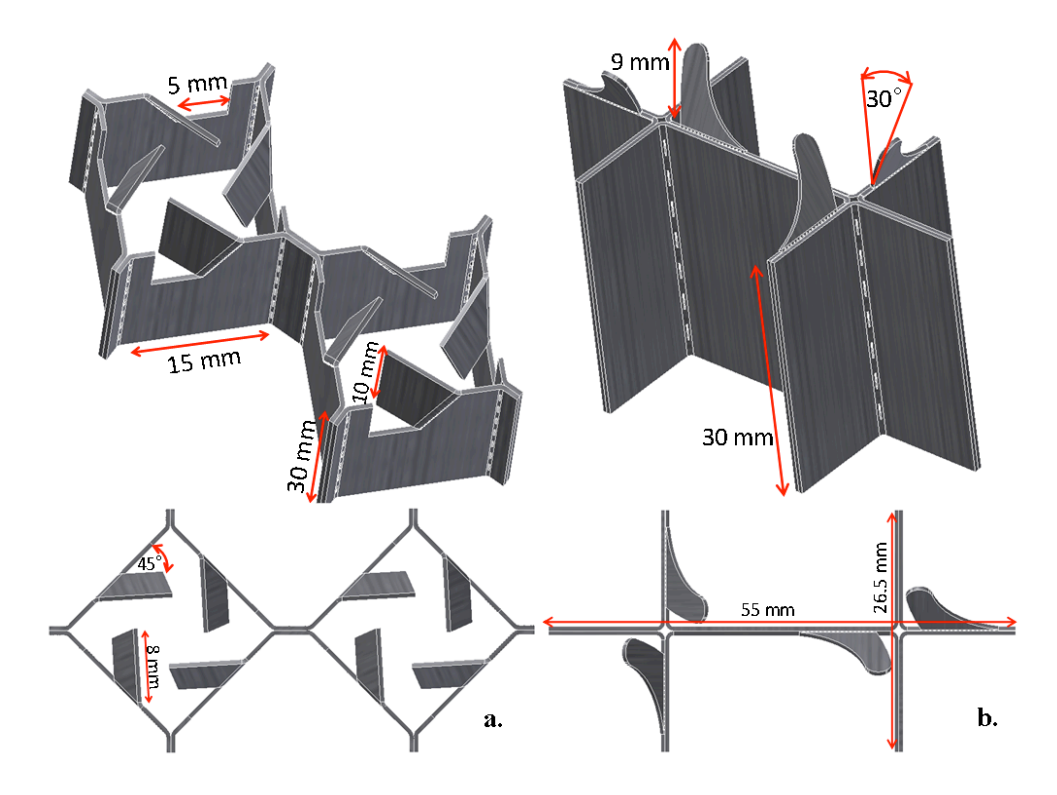


Figure 3 The two spacer designs, Spacer 1 (a) and Spacer 2 (b), examined in this study.

1.2 The Rossendorf Ultrafast Electron Beam X-ray Tomograph

The Rossendorf Ultrafast Electron Beam X-ray Tomograph (ROFEX) facility is a leading imaging device in terms of time resolution. The high frame rate imaging is achieved by applying the scanned electron beam principle featuring a quickly moving X-ray emitting spot scanning the steady specimen placed into the middle of the tomograph [17], [18]. A tungsten target ring is bombarded from an electron gun by a 150 kV electron beam with a maximum beam current of 65 mA as is shown in Figure 4a. The beam is focused and scanned very fast over the tungsten target producing an X-ray emitting spot of about 1 mm diameter. The maximum beam-sweep frequency is 10 kHz. The detector ring comprises 240 room temperature semiconductor pixels of 1.33mm x 1.33mm size. This combination enables a spatial resolution of 0.51 lp/mm at 10% value of the modulation transfer function (MTF) [17]. The detector is arranged at a slight axial offset of 3mm relative to the plane of the focal spot path. Scanning of an object occurs in a single computed tomography (CT) plane. The maximum imaging rate is given as 7000 fps [17]. Note that due to the horse-shoe shaped tungsten target a full 360° projection of the specimen is not possible, however this is not influencing the quality of the imaging as the minimal necessary projection angle (180° + fan beam angle [21]) is achieved. Further details about the ROFEX tomograph can be obtained from [17], [18].

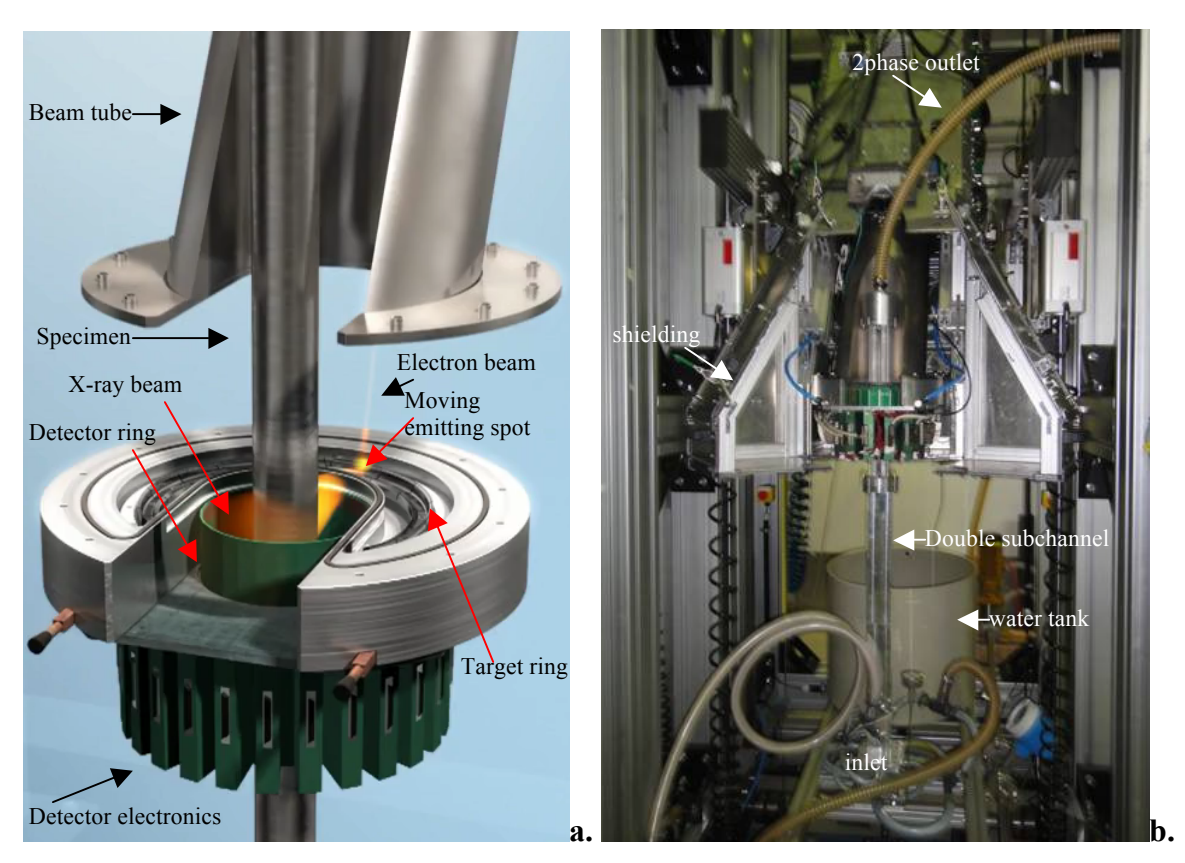


Figure 4 Illustration of the operating principle of the ROFEX tomograph (a) and a photo of it with the double subchannel inside it (b).

2. Experimental conditions

A large number of experiments (about 70) have been carried out changing the flow conditions and imaging the empty channel or the channel with a spacer in it. The present paper shows only a selection of few tests to illustrate the results. Due to the limited spatial resolution of the imaging, we have deliberately chosen flow conditions that manifest quite thick liquid films (see Table 1).

Furthermore, we have used a 1.66 M solution of NaI and water instead of pure water in order to increase the contrast resolution of the imaging of the liquid film. Using NaI at such concentration results only in small changes in the liquid properties playing an important role for annular flow as is shown in Figure 5. However it significantly increases the X-ray attenuation of the liquid with respect to the aluminum walls. Note that an electron beam current of 14 mA has been used for all tests.

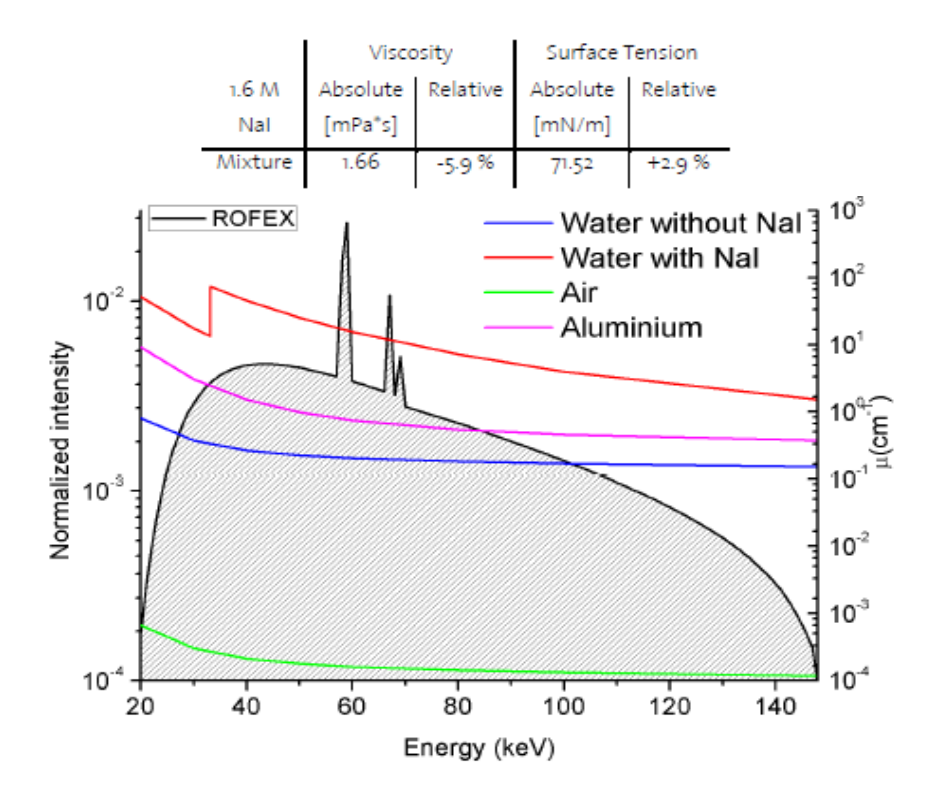


Figure 5 150kV tungsten X-ray spectrum and the linear attenuation coefficients of the different materials present in the flow loop. Adding NaI contrast agent to the water at 1.66 M does not change much the liquid properties with respect to pure water (table at top).

All tests were carried out at ambient temperature of approximately 20 °C. It is usual to describe the two-phase flow by the superficial gas and liquid velocities:

$$J_g = \frac{\dot{V}_g}{A} \text{ and } J_1 = \frac{\dot{V}_1}{A}, \qquad (1)$$

where A is the channel cross section and \dot{V} is the volumetric flow rate. Further, the gas volume flow fraction is defined as:

$$\beta = \frac{\dot{V}_g}{\dot{V}_g + \dot{V}_l} \,. \tag{2}$$

The experimental conditions are summarized in Table 1. Note that for the same air-water flow rates the presence of the spacer inside the channel results in a pressure increase at the inlet of the channel of less than 0.05 bar. The imaging rate was 2000 fps and a measurement typically took 3s. For each measurement series with a certain geometry (with or without spacer, axial position etc.) or flow condition two reference measurements have been performed: one with an empty channel and one with the channel filled with water.

Table 1: Experimental conditions

	Air flow [Nm3/h]	Water flow [l/h]	J _{air} [m/s]	J _{water} [m/s]	1-β	P inlet [bar]	Other parameters
							No spacer
Exp 1	90.3	1670	13.87	0.598	0.0413	2.45	Spacer 1 Spacer 2

3. Determining liquid film thickness and average void fraction

The water-filled reference and the actual measurements are reconstructed using the fan-beam reconstruction algorithm [21] on a 128×128 pixel grid using a Hamming window smoothed ramp filter into non-scaled grey values based on the empty reference. Using an appropriate region of interest (ROI) inside the channel for the reconstructed water reference, the grey value corresponding to pure water, $p_{water,ref}$ is obtained by averaging over the ROI. The same is done to get the pure-air grey level based on a ROI outside of the channel for the water reference, $p_{air,ref}$ and for each actual reconstructed two-phase measurement, p_{air} . As there is usually slight offset between $p_{air,ref}$ and p_{air} , the pure water value for the actual measurement is scaled as:

$$p_{water} = \frac{p_{air}}{p_{air,ref}} p_{water,ref}. \tag{3}$$

The void fraction or more precisely the liquid hold up for a pixel with grey level p is obtained then as:

$$\varepsilon = \frac{p - p_{water}}{p_{water} - p_{air}}. (4)$$

The liquid film thickness (LFT) can be determined, assuming that the liquid signal near the wall belongs to waves (not to droplets) and can therefore be considered part of the liquid film, as follows [16]:

$$LFT = \int_{0}^{x_{\text{max}}} \varepsilon(x) dx, \qquad (5)$$

where the integral is taken over radial lines such as shown in yellow in Figure 6a. Note that on this image only those pixels where some liquid is (partially) present should have a nonzero value. Some lighter regions outside of the channel are due to inaccuracies in the referencing (see below in Section 4) and reconstruction artefacts. Typical profiles of ε over a yellow line in the region of the liquid film are shown in Figure 6b. It shows that the peak in this profile is quite broadened, smeared out. In case of the time-averaged profile it is due partly to the limited spatial resolution of the imaging (certainly not better than 1 mm as is explained above) that results in blur. The other effect contributing to smearing is the temporal averaging of an oscillating film thickness. The extent and influence of the oscillations are illustrated by showing two instantaneous profiles also in Figure 6b. Note that the profiles shown in the figure are obtained for the right half pin in Figure 6a at around 90 degree polar angle in the subchannel gap between the pins. Due to the smearing some care has to be taken in choosing the actual integration limits in eq. (5). We choose the lower integration limit at the position where the signal first hits zero starting from the peak in the profile towards the wall. The upper integration limit, x_{max} , that should ideally correspond to the maximal wave height at the given polar coordinate, is taken where ε first decreases to the level of the average liquid hold up in the gas core (see Figure 6b). This latter value is estimated again by taking an average over an

appropriate ROI. Note that the pixel resolution of the reconstructed images is estimated based on the known geometry of the double subchannel to be 0.54mm/pixel. Note that even at a spatial resolution that seems to be limited in comparison to the average liquid film thickness (see Figure 7 below), eq. (5) still allows determining the LFT. Nevertheless the accuracy of it still needs to be assessed. Note that similar evaluation of the LFT based on cold neutron imaging yielded 7-10% accuracy though the spatial resolution was higher (around 350µm) in that case [15], [16].

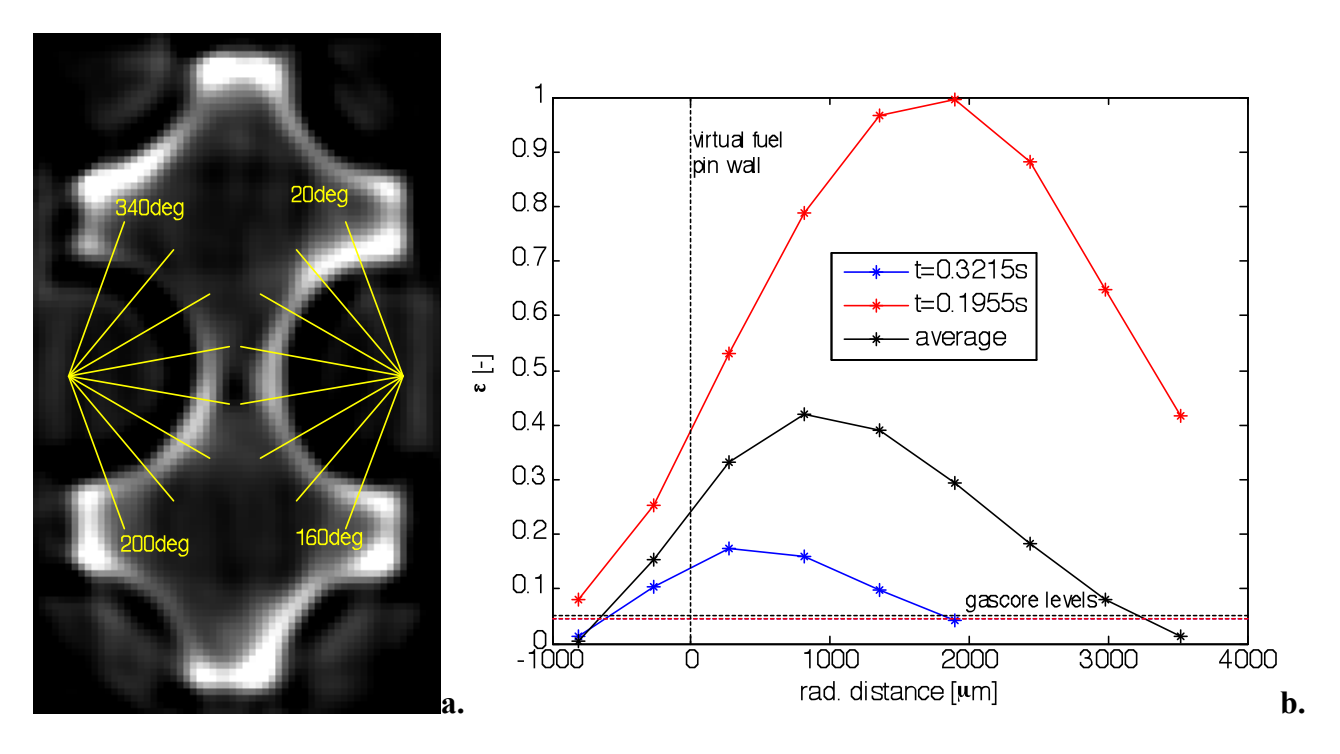


Figure 6 Reconstructed image of the time-averaged liquid hold up distribution over the channel cross section for a measurement 3.5 cm above the vanes of Spacer 2 (a). Period of averaging is 3s. The pixel values are converted to liquid hold up here according to eq. (4). A typical liquid hold up profiles for the right half pin over a yellow line at around 90 degree shown in the reconstructed image (b). The time-average profile and two instantaneous profiles are shown. The corresponding liquid hold up levels in the gas core are shown by horizontal dashed lines.

The distribution of the time-averaged LFT along the perimeter of the two half pins about 3.5 cm above the tip of the vanes of Spacer 2 is shown in Figure 7. Note the water pooling in the corners of our geometry in Figure 6a. For this reason we do not evaluate the LFT on the half pin close to the corners. The first and last 20 degrees are always ignored. The quite high values at around 30 degree for the right half pin can be still slightly influenced by the water pooling. The strong non-uniformity of the LFT along the pin perimeter is introduced by the effect of the spacer vanes. The distribution resembles very much to those shown in [15] and [16] for thinner films. Fore a more detailed analysis on the influence of the spacers on the time-averaged LFT see [16].

Figure 6 has already shown that significant temporal oscillations in the profile of the liquid film are measured that are due to waves crossing the CT plane. This is further illustrated in Figure 8a showing the LFT oscillations at three different polar positions (two in the directions of the two subchannel centers, one in the subchannel gap) on the surface of the right half pin. The corresponding power spectra of the LFT oscillations are shown in Figure 8b. In the 10-30 Hz frequency range one can notice relatively high power content in the oscillations. The inset in Figure

8b shows an estimate of the probability density function (PDF) of the LFT at the three aforementioned angular positions. The highest average LFT value of the three, belonging to 92 degrees (see also Figure 7), corresponds also to the highest value of the position of the peak and the centre of gravity of these distributions. Note that these PDFs are not the same as the distribution of the wave amplitudes, nevertheless examining them together with the time traces one can state that the waves in the liquid film are the largest in general at 92 degrees, i.e. in the subchannel gap between the pins. Whereas at e.g. 132 degrees the waves are in general significantly smaller and very large waves are much less frequent. Furthermore the distribution at 92 degrees, unlike the other two, tends to be bi-modal.

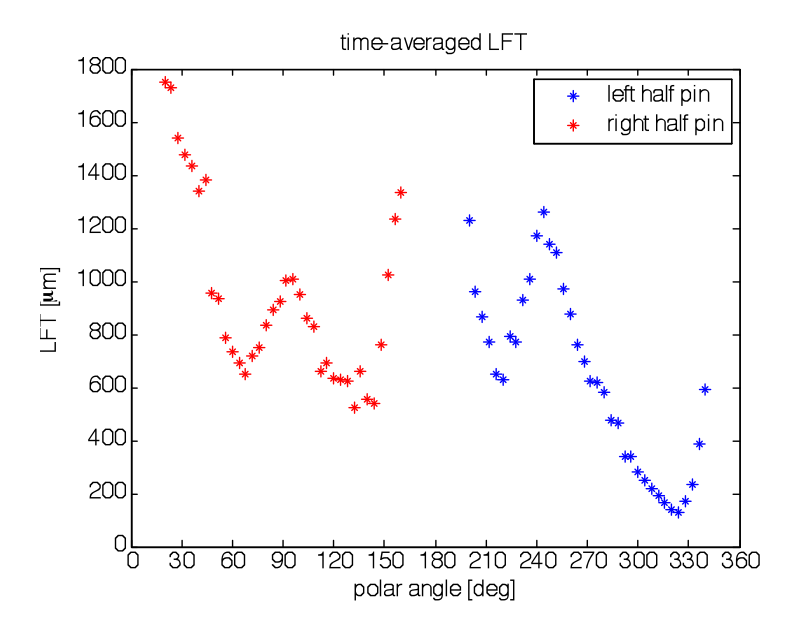


Figure 7 The angular distribution of the time-averaged LFT 3.5 cm above the vanes of Spacer 2 on the two half pin surfaces at the height of the CT plane.

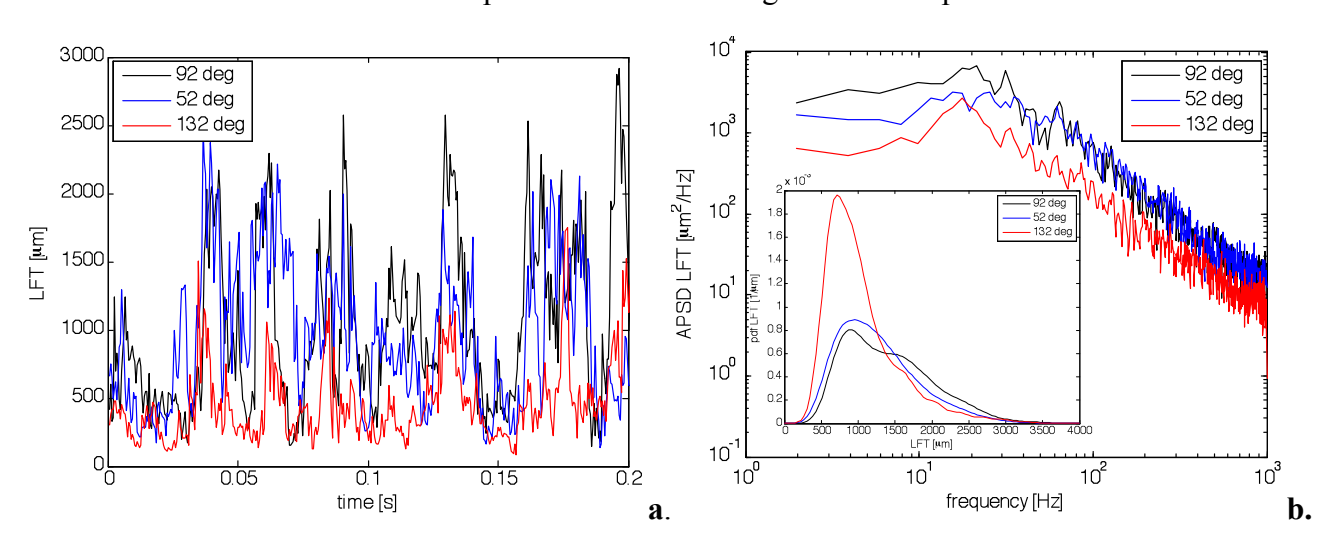


Figure 8 The time dependence of the LFT at three polar angles on the surface of the right half pin (see Figure 6a) (a). The power spectrum of LFT oscillations (b). The inset shows the probability density function of the LFT.

We have also estimated the cross-sectional averaged liquid hold up, $\langle \varepsilon \rangle$, again by averaging over an appropriate ROI confining the inner channel cross section. The time variation of this quantity is shown in Figure 9a. Note that the average void fraction in the channel is just 1- $\langle \varepsilon \rangle$. The power spectrum of $\langle \varepsilon \rangle$ is shown in Figure 9b. This exhibits even more prominently as in Figure8b a "peaking" in the 10-30 Hz range. This is the range of characteristic frequencies at which the larger waves that influence the cross-sectional averaged void fraction, travel through the channel.

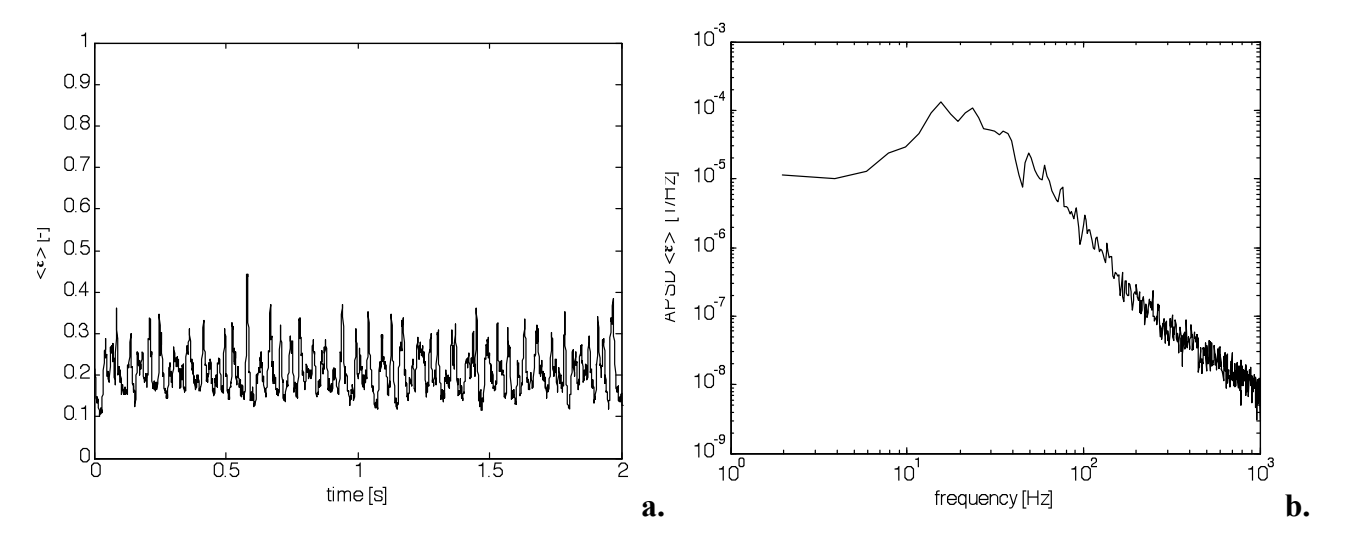
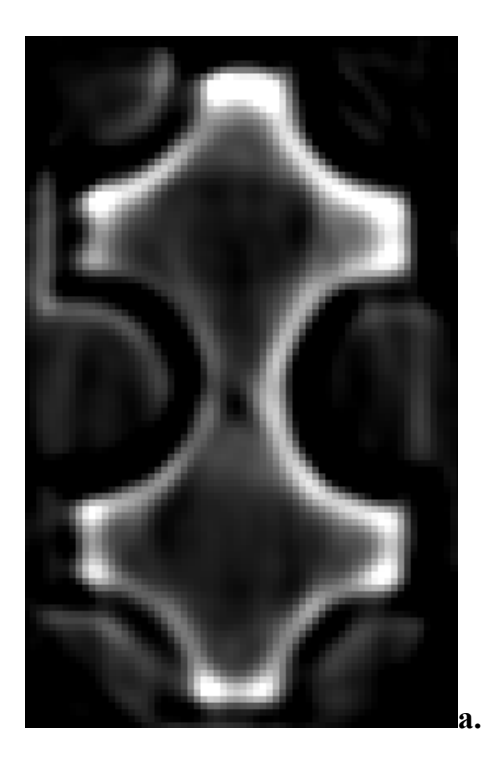


Figure 9 The time dependence of the cross-sectional averaged liquid hold up (a.) The corresponding power spectrum (b.)

4. Sensitivity of reconstructing the liquid film

In the previous section a short overview of the annular flow parameters that can be determined based on the X-ray imaging in the ROFEX facility has been given. A case with Spacer 2 has been shown there. Examining other measurement series, we have found that the imaging shows a very high degree of sensitivity to the accuracy of the referencing. If a little mismatch/offset is present between the reference and the actual measurements artefacts appear in the reconstructed image and strongly influence e.g. the estimation of the LFT. This is obviously a consequence of imaging liquid films that are relatively thick though still not thick enough for the limited spatial resolution. Two examples are shown in Figure 10, both obtained for the same flow condition as is given in Table 1. Figure 10a, a measurement without spacer in the channel, shows especially strong shadow artefacts (the outer edge of the channel wall should be invisible) due to mismatch between the reference and the actual measurements. The channel cross section does not look symmetrical as it is in Figure 6a and the liquid film on the left half pin is clearly very much affected by this (hardly observable) and cannot be measured reliably at all. Note that for Figure 10a the reference measurements have not been performed directly before or after the actual measurements but only later. Therefore tiny uncertainties in reproducing the exact height of the CT plane might play a role in having a mismatch as well. The case for Figure 10b, showing the measurement above Spacer 1, is however different as the references have been directly measured before the actual measurement. The artefacts, however, though less severe as in Figure 10a, are also present. Note also that based on the images above the mismatch seems not to be only a shift but some rotation or skew seems to occur as well. These indicate that minute distortions in the actual path of the X-ray emitting spot with respect to the expected one might be responsible for the mismatch. Great care is taken to form very precisely and to monitor the actual emitting spot path (for details see [17], [18]). Nevertheless other effects that are more difficult to control like small differences due to thermal expansion of the target ring - though it is cooled efficiently to dissipate the about 2kW power it is exposed to - during the reference measurement and the actual measurement might be responsible for minuscule distortions.

Nevertheless, it will be attempted in the future to compensate for the aforementioned mismatch between reference and actual measurement in the post processing phase which should be feasible. If this effort is successful, one can proceed with quantifying the effect of the spacers on the different annular flow parameters obtained in the previous section.



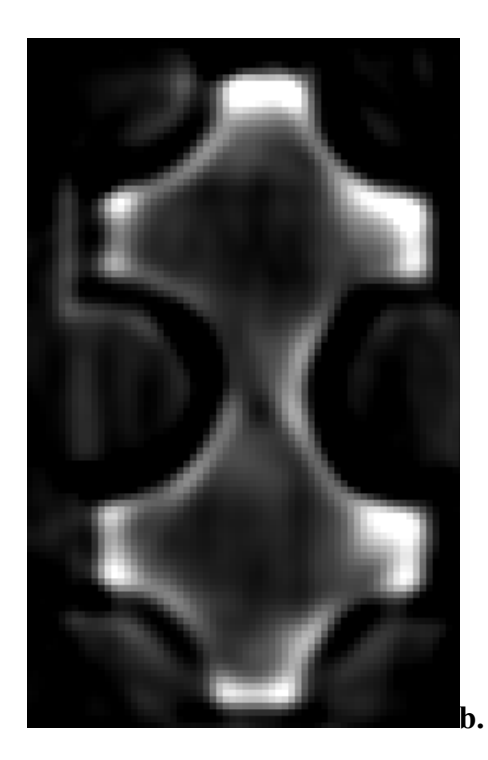


Figure 10 Reconstructed image of the time-averaged liquid hold up distribution in the channel for a measurement without spacer (a). Reconstructed image of the time-averaged liquid hold up distribution for a measurement about 3.5 cm above the vanes of Spacer 1 (b.)

5. Conclusions

The feasibility of using ultra-fast X-ray tomography at the ROFEX facility for studying annular flows in a double subchannel model of a BWR fuel bundle has been examined. It has been demonstrated that even though the spatial resolution of the device is somewhat limited in comparison to the average film thickness, thick liquid films can be studied successfully. Quantities like the liquid film thickness distribution along the perimeter of the virtual fuel pins have been determined. The high time resolution of the imaging enables to resolve the wavy structure of the liquid film. Spectral analysis shows that the characteristics frequency of the waves passing by is in the range of 10-30 Hz. The probability density of the film thickness indicates that the wave height and its distribution vary significantly with the angular position on the pin surface. This first evaluation shows the feasibility of ultra-fast X-ray tomography to study annular flows and liquid films. A strong sensitivity to minute mismatches between the reference and the actual measurements has been found, however. Compensating or reducing such effects will be examined in a future research effort.

6. References

- [1] R.T. Lahey and F.J. Moody, "The Thermal-Hydraulics of a Boiling Water Nuclear Reactor", 2nd Ed. La Grange Park, IL: American Nuclear Society, 1993.
- T. Gustafsson, "Fuel assembly and spacer for a boiling reactor" U.S. Patent #5,530,729 Issued Jun 25, 1996.
- [3] D.G. Smith, J.E. Maynard, "Spacer and fuel assembly for a nuclear reactor. U.S. Patent #6,507,630 issued Jan 14, 2003.
- [4] O. Nylund, "Spacer and fuel assembly for a nuclear reactor", U.S. Patent #6,816,563 issued Nov 9, 2004.
- [5] S. Helmersson, L. Larsson, O. Nylund, H. Söderberg, "A spacer and a fuel unit for a nuclear plant", Europen Patent # EP 1 706 874 B1, issued 09.12.2009.
- [6] W. Kraemer, G. Proebstle, W. Uebelhack, T. Keheley, K. Tsuda, S. Kato, "The ULTRAFLOW spacer an advanced feature of ATRIUM fuel assemblies for boiling water reactors", Nucl. Eng. Des.,154, 1995, pp. 17-21.
- [7] G. Feldhaus, B.J. Azzopardi, W. Zeggel, "Annular flow experiments in rod bundles with spacers", Nucl. Eng. Des., 213, 2002, pp. 199-207.
- [8] M. Glück, Validation of the sub-channel code F-COBRA-TF Part I. Recalculation of single-phase and two-phase pressure loss measurements", Nucl. Eng. Des. 238, 2008, pp. 2308-2316.
- [9] M. Glück, "Validation of the sub-channel code F-COBRA-TF Part II. Recalculation of void measurements", Nucl. Eng. Des., 238, 2008, pp. 2317-2327.
- [10] M. Damsohn, H.-M. Prasser, "Experimental studies of the effect of functional spacers to annular flow in subchannels of a BWR fuel element", Nucl. Eng. Des., 240, 2010, pp. 3126-3144.
- [11] Shirakawa, N., Yamamoto, Y., Horie, H., Tsunoyama, S. 2002. Analysis of flows around a BWR spacer by the two-fluid particle interaction method. J. Nucl. Sci. Eng. Vol **39**, No. 5., pp.572-581.
- [12] M. Damsohn, H.-M. Prasser, "High-speed liquid film sensor for two-phase flows with high spatial resolution based on electrical conductance", Flow Meas. Inst., 20, 2009, pp. 1-14.
- [13] Kureta, M., 2007a. Development of a neutron radiography three-dimensional computed tomography system for void fraction measurement of boiling flow in tight lattice rod bundles. Journal of Power and Energy Systems, **1**(3), pp.211-224.
- [14] Kureta, M., 2007b. Experimental study of three-dimensional void fraction distribution in heated tight-lattice rod bundles using three-dimensional neutron tomography. Journal of Power and Energy Systems, 1(3), pp.225-238.
- [15] Kickhofel, J., Zboray, R., Damsohn, M., Kaestner, A., Lehmann E., Prasser, H.-M., 2011. Cold neutron tomography of annular coolant flow in a double subchannel model of a boiling water reactor. To appear in Nucl. Inst Meth. A. doi:10.1016/j.nima.2011.01.062.

The 14th International Topical Meeting on Nuclear Reactor Thermalhydraulics, NURETH-14 Toronto, Ontario, Canada, September 25-30, 2011

- [16] R. Zboray, J. Kickhofel, M. Damsohn, H.-M. Prasser, "Cold-neutron tomography of annular flow and functional spacer performance in a model of a Boiling Water Reactor fuel rod bundle", 2011 To appear in Nucl. Eng. Des.
- [27] F. Fischer, D. Hoppe, E. Schleicher, G. Mattausch, H. Flaske, R. Bartel, U. Hampel, "An ultra fast electron beam x-ray tomography scanner", Meas. Sci. Technol., 19, 2008, 094002.
- [18] F. Fischer, U. Hampel, "Ultra fast electron beam X-ray tomography for two-phase flow measurement", Nucl. Eng. Des., 240, 2010, pp. 2254-2259.
- [19] M. Bieberle, F. Fischer, E. Schleicher, H.J. Menz, H.-G. Mayer, U. Hampel, "Experimental two-phase flow measurement using ultra fast limited-angle-type X-ray computed tomography", Exp. Fluids, 47, 2009, pp. 369-378.
- [20] M. Bieberle, F. Fischer, E. Schleicher, H.J. Menz, H.-G. Mayer, U. Hampel, "Dual-plane ultrafast limited-angle electron beam X-ray tomography", Flow Meas. Inst., 21, 2010, pp. 233-239.
- [21] A. C. Kak, M. Slaney, 2001. Principles of Computerized Tomographic Imaging. Society of Industrial and Applied Mathematics.
- [22] G. F. Hewitt, N.S. Hall-Taylor, 1970. Annular two-phase flow. Pergamon, Oxford, UK.